INTERNATIONAL JOURNAL FOR NUMERICAL METHODS IN FLUIDS
Int. J. Numer. Meth. Fluids 2004; **44**:1207–1229 (DOI: 10.1002/fld.682)

Three-dimensional incompressible flow calculations using the characteristic based split (CBS) scheme

P. Nithiarasu*,†, J. S. Mathur‡, N. P. Weatherill and K. Morgan

Civil and Computational Engineering Centre, School of Engineering, University of Wales Swansea, Swansea SA2 8PP, U.K.

SUMMARY

In this paper, the characteristic based split scheme is employed for the solution of three-dimensional incompressible viscous flow problems on unstructured meshes. Many algorithm related issues are discussed. Fully explicit and semi-implicit forms of the scheme are explained and employed in the calculation of both isothermal and non-isothermal incompressible flows simulation. The extension of the scheme to porous medium flows is also demonstrated with relevant examples. Copyright © 2004 John Wiley & Sons, Ltd.

KEY WORDS: CBS scheme; explicit; semi-implicit; incompressible flow; porous media flow; artificial compressibility; velocity correction

1. INTRODUCTION

The solution of incompressible flow problems is important in a range of applications including heat exchanger design, low speed aerodynamics, hydrodynamic systems, cooling of electronic systems and bio-medical systems. It is increasingly important to be able to deal with complicated geometries in these applications. For this reason, although structured and semi-unstructured meshes are widely employed in incompressible flow applications, the need for accurate and efficient unstructured mesh solvers is becoming apparent. In this paper, the generality and validity of the characteristic based split (CBS) code, a multi purpose Navier–Stokes solver, is discussed in the context of incompressible viscous flows. Several examples are presented to demonstrate the accuracy and efficiency of this unstructured based flow solver.

*Correspondence to: P. Nithiarasu, Civil and Computational Engineering Centre, School of Engineering, University of Wales Swansea, Swansea SA2 8PP, U.K.
†E-mail: P.Nithiarasu@swansea.ac.uk
‡On leave from Computational & Theoretical Fluid Dynamics Division National Aerospace Laboratories, P.B. 1779, Bangalore 560 017, India.

Contract/grant sponsor: EPSRC; contract/grant number: GR/R29321/01

Received 13 January 2003
Revised 24 November 2003

Unstructured mesh methods for compressible flow are very well developed and there are several schemes that enable large scale computations to be performed [1–10]. The success of these schemes is partially due to explicit time discretization of the equations along with dual time stepping. The addition of extra dissipation to smooth oscillations is generally part of these schemes. These schemes perform well for very high speeds but the solvers become inefficient for low speed flows due to severe time step limitations at small and moderate Reynolds numbers. Therefore, alternative approaches have been developed to solve incompressible flows. The projection, or velocity correction, schemes and preconditioned artificial compressibility schemes are two such methods which are capable of handling a wide range of Reynolds numbers. However, many velocity correction based schemes require some form of implicit solution of the pressure Poisson equation [11–24], so that the use of these schemes needs very efficient simultaneous equation solvers and may require large memory for three-dimensional problems.

The CBS method [16–25] for incompressible flows is a variant of the velocity correction method or split method reported by many authors [11–15]. However, the CBS procedure is efficient and flexible due to extra provisions which lead to improved stability and accuracy of incompressible flow calculations. Incompressible flow calculations performed previously with the CBS scheme were mainly based on either semi- or quasi-implicit forms in which some form of implicit solution is necessary. However, recently it has been proved that the artificial compressibility (AC) and the CBS schemes can be combined to get an efficient and accurate explicit matrix free scheme [25].

This fully explicit scheme was developed by combining the principles of the split scheme and the standard AC scheme [26–30]. Such a scheme gives good pressure stabilization at small and moderate Reynolds numbers and, when combined with characteristic based discretization in the time domain, gives a stable solution for highly convective flows. In addition, an appropriate artificial compressibility parameter and associated local time steps gives faster convergence to steady state. With this type of scheme, a true transient solution is generally achieved via a dual time stepping method [25, 30, 31].

The semi-implicit version is partially implicit due to the requirement for the implicit solution of a pressure Poisson equation. Here pressure and convection stabilization are achieved in a manner similar to that employed for the fully explicit form but no AC is used. In flows dominated by source terms, the semi-implicit form is found to perform better than the fully explicit form.

The objective of the present paper is mainly to carry out incompressible flow calculations using the CBS scheme on three-dimensional unstructured meshes. Many scheme related issues are also addressed. Several benchmark and application problems have been studied and compared with available data wherever possible.

2. THE NAVIER–STOKES EQUATIONS

The Navier–Stokes equations for a non-isothermal fluid flow can be written in non-dimensional conservative form as

$$\frac{\partial \mathbf{W}}{\partial t} + \frac{\partial \mathbf{F_j}}{\partial x_j} - \frac{\partial \mathbf{G_j}}{\partial x_j} = \mathbf{S} \tag{1}$$

where

$$\mathbf{W}=\begin{pmatrix}\rho\\ \rho u_1\\ \rho u_2\\ \rho u_3\\ \rho T\end{pmatrix},\quad \mathbf{F_j}=\begin{pmatrix}\rho u_j\\ \rho u_1u_j+p\delta_{1j}\\ \rho u_2u_j+p\delta_{2j}\\ \rho u_3u_j+p\delta_{3j}\\ \rho Tuj\end{pmatrix}$$

$$\mathbf{G_j}=\begin{pmatrix}0\\ \tau_{1j}\\ \tau_{2j}\\ \tau_{3j}\\ \dfrac{1}{Re\,Pr}\dfrac{\partial T}{\partial x_j}\end{pmatrix},\quad \mathbf{S}=\begin{pmatrix}0\\ 0\\ 0\\ \rho\dfrac{Gr}{Re^2}T\\ 0\end{pmatrix}$$

These equations represent the conservation of mass, momentum in the three co-ordinate directions and energy, respectively. Here, ρ is the density, x_j are the co-ordinate directions, u_j are the velocity components, t is the time, p is the pressure and T is the temperature. The Reynolds, Prandtl and Grashof numbers are represented by Re, Pr and Gr, respectively, and these are defined as

$$Re=\frac{u_\infty L}{v},\quad Pr=\frac{v}{\alpha},\quad Gr=\frac{g\beta\Delta TL^3}{v\alpha} \tag{2}$$

The remaining non-dimensional scales are standard and used in many text books and papers [9, 31].

In Equation (2) u_∞ is a reference velocity, L is a characteristic dimension, v is the kinematic viscosity, α is the thermal diffusivity, g is the acceleration due to gravity and β is the coefficient of thermal expansion. The non-dimensional form of deviatoric stress is defined by

$$\tau_{ij}=\frac{1}{Re}\left(\frac{\partial u_i}{\partial x_j}+\frac{\partial u_j}{\partial x_i}-\frac{2}{3}\frac{\partial u_k}{\partial x_k}\delta_{ij}\right)$$

where δ_{ij} is the Kronecker delta. The force of gravity acts along the x_3 direction and this is reflected by the inclusion of the buoyancy term in the x_3 momentum equation. Note that, for incompressible flows, density variation can be neglected and the conservation of mass equation becomes an equation to impose the requirement for a divergence free velocity field. However, in artificial compressibility forms, an artificial form of the density variation is retained in the continuity equation.

The isothermal flow solution can be obtained by decoupling the energy equation from the other equations. For forced convection problems, the energy equation may be decoupled from the other equations if only a steady state solution is of interest. Natural convection or transient problems must be solved by using the coupled system of equations. To simulate natural or free convection problems, the Reynolds number in the governing equations is replaced by $1/Pr$ to represent appropriate non-dimensional scale.

3. CHARACTERISTIC BASED SPLIT (CBS) SCHEME

Both explicit and semi-implicit forms of the CBS procedure are employed in this paper. The semi-implicit form needs implicit solution of the pressure Poisson equation. In practice, we find the fully explicit form much easier to handle than the semi-implicit form. However, for problems with large source terms (example: flow through a porous medium), the fully explicit form fails and use of the semi-implicit form is necessary in such situations.

To describe the CBS algorithm and its application to the solution of three-dimensional, incompressible flow problems, we first define the mass flow rate

$$U_j = \rho u_j \tag{3}$$

and rewrite the equation for mass conservation as

$$\frac{\partial \rho}{\partial t} = \frac{1}{c^2}\frac{\partial p}{\partial t} = -\frac{\partial U_j}{\partial x_j} \tag{4}$$

where c is the speed of sound. Each momentum conservation equation is expressed as

$$\frac{\partial U_i}{\partial t} = -\frac{\partial}{\partial x_j}(U_i u_j) - \frac{\partial p}{\partial x_i} + \frac{\partial \tau_{ij}}{\partial x_j} + S_i \tag{5}$$

Note that, for incompressible flows, $c^2 \to \infty$ in Equation (4). However, AC schemes use finite values for c^2 calculated from velocity and temperature fields [25, 31] as discussed in Section 4.

The CBS procedure has been the subject of research for the last 8 years and the basic algorithm is available in many earlier publications [9, 16–25]. Briefly, the characteristic procedure is based on particle backtracking in the time–space domain, avoiding the need to resort to moving co-ordinates. For accuracy, it is necessary to integrate backwards exactly, an expensive and complicated procedure. A temporal Taylor expansion makes this tractable. This backward approximation results in extra, consistent, second-order stabilizing terms, which stabilize the scheme by suppressing oscillations generated from the discretization of convection terms. In order to make use of the characteristic property, the governing Navier–Stokes equation system is split into a series of fractional stages. The momentum components are discretized in time using this procedure as,

$$\begin{aligned} U_i^{n+1} - U_i^n = \Delta t \left[-\frac{\partial}{\partial x_j}(U_i u_j)^n - \frac{\partial p^{n+\theta_2}}{\partial x_i} + \frac{\partial \tau_{ij}^n}{\partial x_j} + S_i^n \right] \\ + \frac{\Delta t^2}{2} u_k \frac{\partial}{\partial x_k}\left(\frac{\partial}{\partial x_j}(U_i u_j)^n + \frac{\partial p^n}{\partial x_i} - S_i^n \right) \end{aligned}$$

where the pressure term is not treated explicitly but is evaluated at a time $t^n + \theta_2 \Delta t$. The notation

$$\frac{\partial p^{n+\theta_2}}{\partial x_i} \equiv \theta_2 \frac{\partial p^{n+1}}{\partial x_i} + (1-\theta_2)\frac{\partial p^n}{\partial x_i} \tag{6}$$

is adopted, where $0 \leqslant \theta_2 \leqslant 1$ ($\theta_2 = 0$ for the fully explicit scheme and $\theta_2 > 0$ for the semi-implicit scheme). In Equation (6), the extra higher order terms are the result of the characteristic based time discretization.

For the solution of these equations, the CBS algorithm uses a fractional step approach with a split. The four steps can be described as

(1) solve the momentum equation without the pressure terms,
(2) calculate the pressure from a Poisson equation,
(3) correct the velocities,
(4) calculate any additional scalar variables, such as temperature, concentration etc., from the appropriate governing equations.

In the first step, we define a new variable U_i^* such that

$$U_i^* - U_i^n = \Delta t \left[-\frac{\partial}{\partial x_j}(U_i u_j)^n + \frac{\partial \tau_{ij}^n}{\partial x_j} + S_i^n \right] + \frac{\Delta t^2}{2} u_k \frac{\partial}{\partial x_k}\left(\frac{\partial}{\partial x_j}(U_i u_j)^n - S_i^n \right) \tag{7}$$

This represents the first part of the split and is explicit. The corrected velocities can be determined, once the pressure is known, using the equation

$$U_i^{n+1} - U_i^* = -\Delta t \frac{\partial p^{n+\theta_2}}{\partial x_i} + \frac{\Delta t^2}{2} u_k \frac{\partial}{\partial x_k}\left(\frac{\partial p^n}{\partial x_i} \right) \tag{8}$$

The solution of this equation is actually the third step in the algorithm. The second step is the determination of the pressure. Referring to Equation (4), we can write

$$\left(\frac{1}{c^2} \right)^n (p^{n+1} - p^n) = -\Delta t \frac{\partial U_i^{n+\theta_1}}{\partial x_i} \tag{9}$$

Now $U_i^{n+\theta_1} \equiv \theta_1 U_i^{n+1} + (1-\theta_1) U_i^n$ where $0.5 \leqslant \theta_1 \leqslant 1$, and using Equation (8) we can write

$$U_i^{n+\theta_1} = \theta_1 \left[U_i^* - \Delta t \frac{\partial p^{n+\theta_2}}{\partial x_i} \right] + (1-\theta_1) U_i^n \tag{10}$$

The higher order terms are neglected in the above equation. Now Equation (9) can be written as

$$\begin{aligned} \left(\frac{1}{c^2} \right)^n (p^{n+1} - p^n) = & -\Delta t \left[\theta_1 \frac{\partial U_i^*}{\partial x_i} + (1-\theta_1) \frac{\partial U_i^n}{\partial x_i} \right] \\ & + \Delta t^2 \theta_1 \left[\theta_2 \frac{\partial^2 p^{n+1}}{\partial x_i \partial x_i} + (1-\theta_2) \frac{\partial^2 p^n}{\partial x_i \partial x_i} \right] \end{aligned} \tag{11}$$

The fourth step of the algorithm involves the calculation of the temperature field using the equation for conservation of energy. Referring to Equation (1), this can be written in the form

$$\frac{\partial}{\partial t}(\rho T) + \frac{\partial}{\partial x_j}(\rho T u_j) - \frac{\partial}{\partial x_j}\left(\frac{1}{Re\, Pr} \frac{\partial T}{\partial x_j} \right) = 0 \tag{12}$$

and, assuming incompressible flow, characteristic time discretization gives

$$T^{n+1} - T^n = \Delta t\left[-\frac{\partial}{\partial x_j}(Tu_j)^n + \frac{\partial}{\partial x_j}\left(\frac{1}{Re\,Pr}\,\frac{\partial T^n}{\partial x_j}\right)\right] + \frac{\Delta t^2}{2}\,u_k\,\frac{\partial}{\partial x_k}\left[\frac{\partial}{\partial x_j}(Tu_j)^n\right] \tag{13}$$

The resulting equations are solved using a standard Galerkin finite element procedure. The computational domain is discretized using a mesh of tetrahedral elements. Within each tetrahedron, the approximation

$$U_i = \sum_{n=1}^{4} N_n \bar{U}_i|_n \tag{14}$$

is adapted, where $n = 1$–4 represent the four vertices of the tetrahedron, N_n is the linear shape function at node n and $\bar{U}_i|_n$ is the value of U_i at node n. This is normally written in the more convenient matrix form

$$U_i = \mathbf{N}\,\bar{\mathbf{U}}_\mathbf{i} \tag{15}$$

where the vectors are given by

$$\mathbf{N} = \{N_1 \;\; N_2 \;\; N_3 \;\; N_4\}, \quad \bar{\mathbf{U}}_\mathbf{i} = \begin{Bmatrix} \bar{U}_i|_1 \\ \bar{U}_i|_2 \\ \bar{U}_i|_3 \\ \bar{U}_i|_4 \end{Bmatrix}$$

With a Galerkin weighting, and defining $\Delta U_i^* \equiv U_i^* - U_i^n$, the final matrix form of Equation (7) is written as

$$\mathbf{M}\Delta\bar{U}_i^* = \Delta t[-\mathbf{C}\,\bar{\mathbf{U}}_\mathbf{i} + \mathbf{K}_\tau + \mathbf{F}] + \frac{\Delta t^2}{2}[\mathbf{K}_\mathbf{u}\,\bar{\mathbf{U}}_\mathbf{i} + \mathbf{F}_\mathbf{u}] \tag{16}$$

where

$$\mathbf{M} = \int_\Omega \mathbf{N}^\mathrm{T}\mathbf{N}\,\mathrm{d}\Omega, \quad \mathbf{C} = \int_\Omega \mathbf{N}^\mathrm{T}\,\frac{\partial}{\partial x_j}\,\mathbf{N}u_j\,\mathrm{d}\Omega$$

$$\mathbf{F} = \int_\Omega \mathbf{N}^\mathrm{T} S_i\,\mathrm{d}\Omega, \quad \mathbf{F}_\mathbf{u} = \int_\Omega \mathbf{N}^\mathrm{T}\,u_k\,\frac{\partial}{\partial x_k}\,S_i\,\mathrm{d}\Omega$$

$$\mathbf{K}_\mathbf{u} = \int_\Omega \mathbf{N}^\mathrm{T} u_k\,\frac{\partial}{\partial x_k}\left(\frac{\partial}{\partial x_j}\mathbf{N}u_j\right)\,\mathrm{d}\Omega, \quad \mathbf{K}_\tau = \int_\Omega \mathbf{N}^\mathrm{T}\,\frac{\partial}{\partial x_j}\,\tau_{ij}\,\mathrm{d}\Omega$$

Here Ω represents the entire computational domain. In a similar manner, Equations (11), (8) and (13) can also be solved using the Galerkin procedure. Other publications [16–25] provide full details of this method. It should be noted here that equal order interpolation is employed for all field variables. Equal order interpolation will result in oscillation free solution as long as the time step value calculated is not far from the stability limit (CFL condition). Further discussions on how the CBS scheme allows equal order interpolation may be found in References [9, 16].

3.1. Extension to porous medium flows

Historically, a number of models have been used for the solution of porous media flow problems but these are not generally suitable for all applications. Hence, the recent trend is to develop a more generalized model, which can be used for all types of porous media.

The governing equations for flow in a porous medium, using a generalized model [32–41], can be written in the non-dimensional conservative form

$$\frac{\partial \mathbf{W}}{\partial t} + \frac{\partial \mathbf{F_j}}{\partial x_j} - \frac{\partial \mathbf{G_j}}{\partial x_j} = \mathbf{S} \tag{17}$$

where

$$\mathbf{W} = \begin{pmatrix} \rho \\ \frac{1}{\varepsilon}\rho u_1 \\ \frac{1}{\varepsilon}\rho u_2 \\ \frac{1}{\varepsilon}\rho u_3 \\ \rho T \end{pmatrix}, \quad \mathbf{F_j} = \begin{pmatrix} \rho u_j \\ \frac{1}{\varepsilon^2}\rho u_1 u_j + p\delta_{1j} \\ \frac{1}{\varepsilon^2}\rho u_2 u_j + p\delta_{2j} \\ \frac{1}{\varepsilon^2}\rho u_3 u_j + p\delta_{3j} \\ \rho T uj \end{pmatrix}$$

$$\mathbf{G_j} = \begin{pmatrix} 0 \\ \frac{1}{\varepsilon}\tau_{1j} \\ \frac{1}{\varepsilon}\tau_{2j} \\ \frac{1}{\varepsilon}\tau_{3j} \\ \frac{1}{Re\,Pr}\frac{\partial T}{\partial x_j} \end{pmatrix}, \quad \mathbf{S} = \begin{pmatrix} 0 \\ -Pu_1 \\ -Pu_2 \\ -Pu_3 + \rho\frac{Gr}{Re^2}T \\ 0 \end{pmatrix}$$

The new parameters introduced here are the porosity of the medium, ε, which represents the fraction of the total volume occupied by the voids, and is assumed to be uniform throughout the domain in this study, and the coefficient P defined by

$$P = \frac{Pr}{Da} + \frac{1.75}{\sqrt{150}}\frac{\sqrt{u_k u_k}}{\sqrt{Da}}\frac{1}{\varepsilon^{3/2}} \tag{18}$$

Here Da represents the Darcy number, which is proportional to the permeability of the porous medium, and is defined as $Da = \kappa/L^2$ where κ is the permeability and L is a reference length. These equations reduce to the Navier–Stokes equations when $\varepsilon \to 1$ and $Da \to \infty$, which means that they reduce to the free fluid case when the porosity is 1. These equations can be easily modified to model the flow in a variable porosity medium [36] and double diffusive convection [35].

4. FULLY EXPLICIT SCHEME

A fully explicit form of the CBS algorithm is obtained by substituting $\theta_2 = 0$ and $\frac{1}{2} \leqslant \theta_1 \leqslant 1$ into Equations (8) and (9). Thus, it becomes necessary to solve Equation (8) explicitly with c replaced by an artificial compressibility parameter β. In general, β is calculated from local velocity and temperature distribution and the mesh size, as discussed below. This gives a critical time step $\Delta t = h/(\beta + |u|)$, where h is the local element size.

4.1. The artificial compressibility parameter and local time step

In order to cover the spectrum of flow conditions, it is essential to define a value for β which is not only suitable for different Reynolds numbers, but also should take care of different flow regimes (diffusion and convection dominated) within a problem at a particular Reynolds number. As the β value is local, we need the appropriate local time steps to account for the local stability limits. It is, therefore, essential to include local time step calculations as part of the scheme.

In this work, the relation

$$\beta = \max(\varepsilon, v_{\text{conv}}, v_{\text{diff}}, v_{\text{therm}}) \tag{19}$$

is employed, where ε is a constant, taken here to be 0.5, v_{conv} is the convective velocity, v_{diff} is the diffusion velocity and v_{therm} is the thermal velocity. These velocities are calculated from the non-dimensional relations

$$v_{\text{conv}} = \sqrt{u_i u_i}, \quad v_{\text{diff}} = \frac{1}{h\,Re}, \quad v_{\text{therm}} = \frac{1}{h\,Pr\,Re} \tag{20}$$

It should be noted that, for pre-conditioned AC schemes, the convection and diffusion velocities are calculated differently [31]. The objective here is to keep the relations as simple as possible, while at the same time ensuring the performance is as good as, or better, than the pre-conditioned scheme. The excellent pressure and convective stabilization properties of the CBS scheme help in achieving good performance.

The local element size at a node i is defined as

$$h_i = \min(3\text{volume}/\text{opposite face area})_{ie} \tag{21}$$

for the three-dimensional case using four-noded tetrahedral elements. Here, the minimum value is selected among the number of elements, i.e. connected to node i. In terms of non-dimensional quantities the local time step Δt is calculated as

$$\Delta t_{\text{conv}} = \frac{h}{u_{\text{conv}} + \beta} \tag{22}$$

In Equation (22), β is calculated from Equation (19).

The calculated Δt is multiplied by a safety factor varying between 0.5 and 1.0 depending on the problem and mesh used. It is important to note that this is the only parameter that has to be specified in the present study. Determining this factor is generally easy. The approach adopted here is to start with a maximum value and to reduce this value until the scheme starts converging.

5. SEMI-IMPLICIT SCHEME

The CBS algorithm can also be used in its semi-implicit form in which an implicit solution of the pressure equation is necessary. The algorithm is conditionally stable if $\frac{1}{2} \leqslant \theta_1 \leqslant 1$ and $\frac{1}{2} \leqslant \theta_2 \leqslant 1$, with a critical time step $\Delta t = h/(|u|)$. In this study, θ_1 and θ_2 are assumed to be equal to unity for the semi-implicit form with $c \to \infty$. Thus, Equation (11) can be rewritten as

$$\frac{\partial^2 p}{\partial x_i \partial x_i}^{n+1} = \frac{1}{\Delta t} \frac{\partial U^*}{\partial x_i} \tag{23}$$

Note that the transient term in the pressure equation, (11), is neglected as c is assumed to be approaching infinity.

In the case of porous medium flows, the additional porous medium terms are also treated implicitly [37]. The quasi-implicit scheme is similar to the semi-implicit form except that all second-order terms in each equation are also treated implicitly. Details are given elsewhere [9, 14, 41].

6. SIMULATING TRUE TRANSIENT SOLUTIONS USING THE EXPLICIT FORM

To add the true transient term to the momentum equation of an isothermal flow, the CBS procedure allows two approaches. The transient terms can either be added to the first step or to the third step. In this study, it is added to the momentum correction step where real velocity values are calculated (Equation (10)). Addition of a true transient term leads to the modified third step equation

$$U_i^{n+\theta_1} = \theta_1 \left[U_i^* - \Delta t \frac{\partial p^{n+\theta_2}}{\partial x_i} \right] + (1 - \theta_1) U_i^n + \Delta t \frac{\Delta U_{i_\tau}}{\Delta \tau} \tag{24}$$

where $\Delta\tau$ is the real time step. In order to achieve second-order real time accuracy, ΔU_{i_τ} is approximated as

$$\Delta U_{i\tau} = \frac{3U_i^{n+1} - 4U_i^n + U_i^{n-1}}{2} \tag{25}$$

In the above equation, U_i^{n+1} is equal to the nth pseudo time level value within the pseudo time loop. The other two values, U_i^n and U_i^{n-1}, need to be appropriately stored at the start of each real time level.

Over each real time step, the pressure residual is reduced to a prescribed value within the pseudo time step, and here the value 10^{-4} is used. In the case of non-isothermal flows, a similar true transient term is added to energy equation to calculate the time dependent temperature distribution.

7. RESULTS AND DISCUSSION

In this section, the three-dimensional results obtained for three-dimensional isothermal and non-isothermal incompressible flow problems are presented. The results are compared against benchmark solutions wherever possible.

7.1. Isothermal flows

The isothermal results are obtained without including the energy equation.

7.1.1. Flow in a lid-driven cavity. Incompressible flow in a lid-driven cavity is one of the familiar test cases and a benchmark solution is available for comparison. The definition of the problem is standard and involves a cube with the top lid moving with a prescribed velocity. The left, bottom and right side walls are assumed to be solid and are subjected to a no slip condition. The remaining two sides are subjected to symmetric condition, as shown in Figure 1. If the semi-implicit form is used, we need one constant pressure boundary condition, which can be imposed at the mid-point on the bottom surface. However, if the fully explicit form is used, there is no need for any constant pressure conditions. In this paper, the fully explicit scheme has been employed to solve this problem.

Figure 2 shows the unstructured mesh used for the problem. It is apparent that the mesh is refined close to the solid walls. This mesh contains 92 405 nodes and 514 297 linear tetrahedral elements. All meshes used in the paper are generated using the PSUE software [5, 6]. The convergence history of the solution for lid-driven cavity at $Re = 400$ is shown in Figure 3. The residual norm is calculated using

$$\text{Residual} = \sum_{i=1}^{NN} \left[\frac{1}{\beta^2} \left(\frac{p^{n+1} - p^n}{\Delta t} \right) \right]^2 \tag{26}$$

where NN is the total number of nodes. For all steady state problems using the explicit scheme, the above value is reduced to a value below 10^{-5}. Where semi-implicit form is used, L_∞ norm of all the variables are reduced to a value below 10^{-5}.

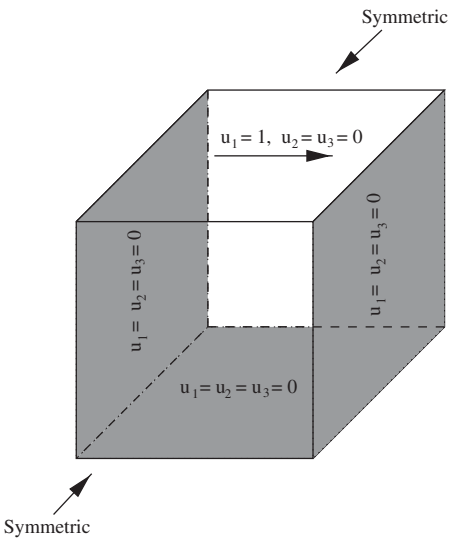

Figure 1. Flow in a lid-driven cavity. Geometry and boundary conditions.

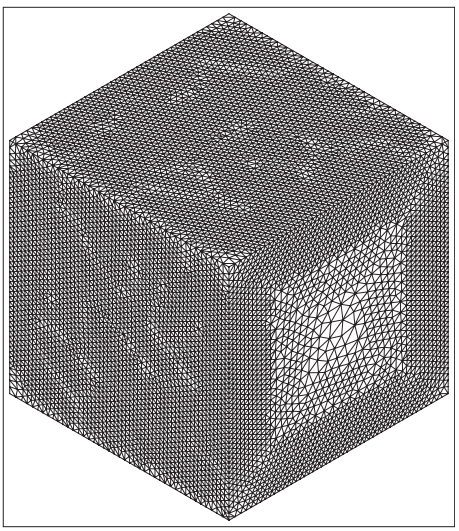

Figure 2. Flow in a lid-driven cavity. Finite element mesh, Nodes: 92 405, Elements: 514 297.

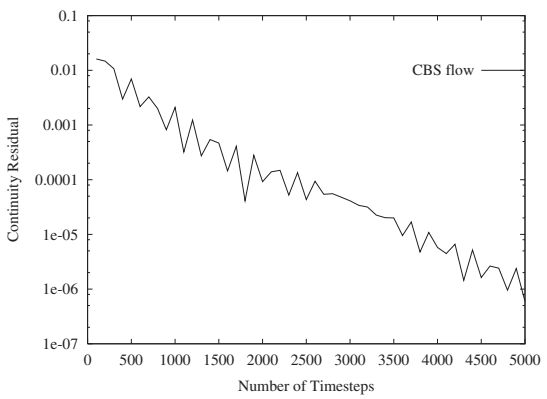

Figure 3. Flow in a lid-driven cavity. Convergence history at $Re = 400$.

The results obtained for the lid-driven cavity at a Reynolds number of 400 are shown in Figure 4. It is apparent that all the contours are smooth and without any appreciable oscillations. In this problem, obtaining a smooth pressure distribution is generally difficult for many numerical schemes due to singularity at the top corners. However, due to effective pressure stabilization of the CBS scheme, the results presented are smooth and stable even close to singular points. The comparison of u_1 velocity distribution along the mid-vertical line with the benchmark solution of Ghia *et al.* [42] is shown in Figure 4(d) and it is apparent that the present results are in excellent agreement with the benchmark solution.

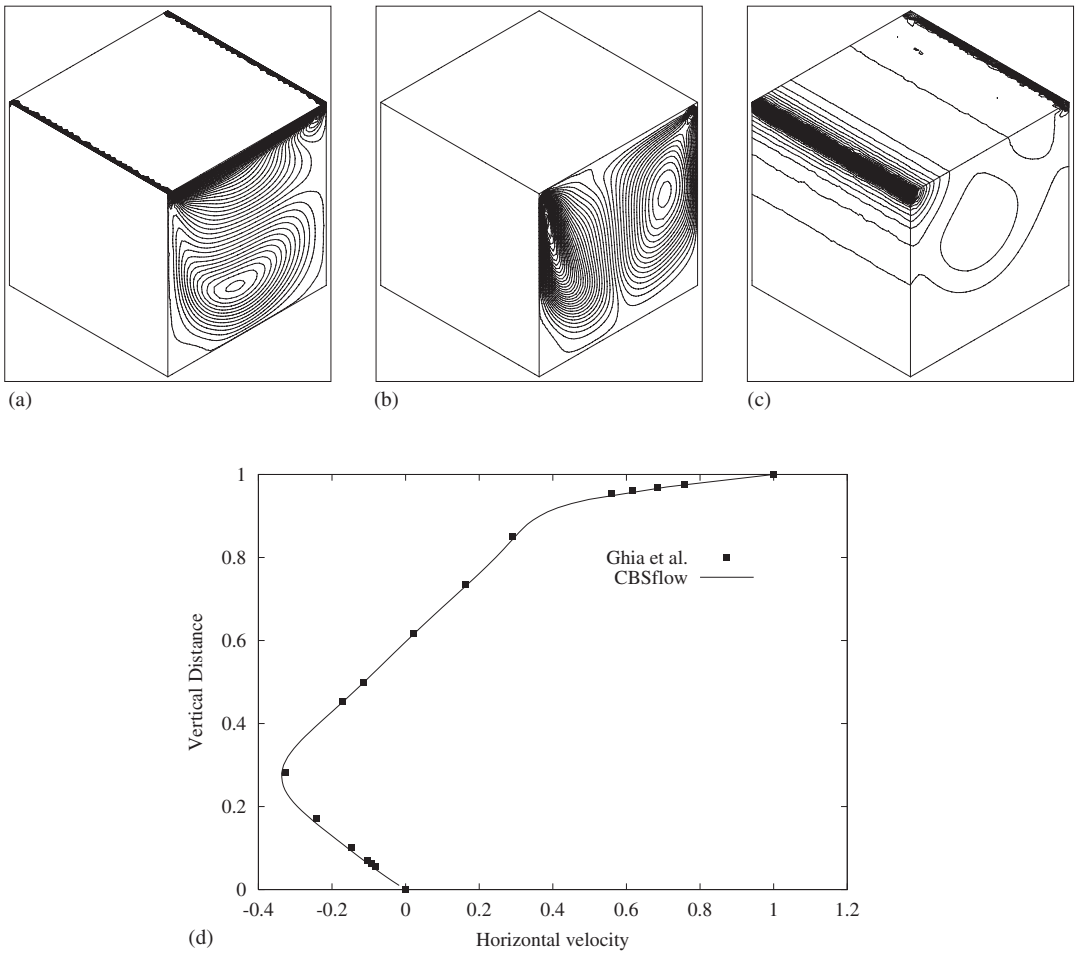

Figure 4. Flow in a lid-driven cavity, $Re = 400$, (a) u_1 velocity contours, (b) u_3 velocity contours, (c) pressure contours, (d) comparison of horizontal velocity distribution along mid-vertical line with Ghia *et al.* [42].

Figure 5 shows a comparison of horizontal velocity distribution along the mid-vertical line with that of Ghia *et al.* [42] for a Reynolds number of 1000. The deviation in the comparisons are expected as Ghia *et al.* results were produced for a two-dimensional geometry. It is also evident from the literature that the unsteady state solution is possible at $Re = 1000$ in three-dimensional driven cavity flows [43]. It is therefore concluded that both three-dimensional and transient effects have contributed to the deviations.

7.1.2. Flow over a backward facing step. The second problem considered is another standard benchmark test case of flow over a backward facing step. The Reynolds number is based on the step height. The inlet section is taken equal to two times the height of the step. The length of the channel ahead of the step is four times the height of the step and the total length of

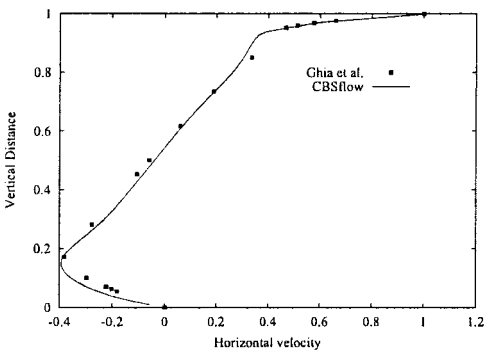

Figure 5. Flow in a lid-driven cavity. Comparison of horizontal velocity distribution along mid-vertical line with Ghia *et al.* [42] at $Re = 1000$.

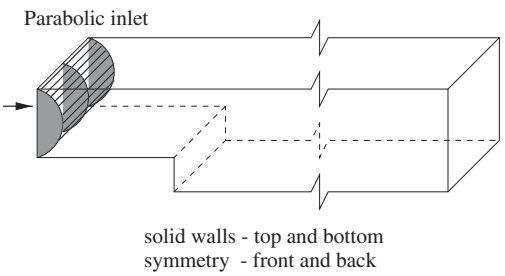

Figure 6. Flow over a backward facing step. Geometry and boundary conditions.

the channel is 40 times the step height. The inlet velocity profile is nearly parabolic and is generated by fitting a curve using the experimental inlet data [43]. Other relevant boundary conditions are shown in Figure 6. The fully explicit form is used for the solution of this problem.

The case considered in this paper has an inlet Reynolds number of 229. For this case, experimental data is available for comparison.

Figure 7 shows the finite element mesh employed and the u_1 velocity contours. The mesh is coarse, with 9686 nodes and 35 436 elements. The contours obtained (Figure 7(b)) are smooth without significant oscillations. The comparison of the velocity distribution with the experimental data is shown in Figure 8. As expected there are some differences but recirculation is predicted excellently. In general, the agreement is good and small deviation is due to the differences in the velocity profile used between the experiment and assumed numerical data.

7.1.3. Flow past a sphere. The next problem considered involves flow past a sphere in a confinement. The computational domain is a rectangular box of length $25D$, where D is the diameter of the sphere, with the downstream boundary located $20D$ from the centre of the sphere. The four side walls are located at a distance of $5D$ from the centre of the sphere.

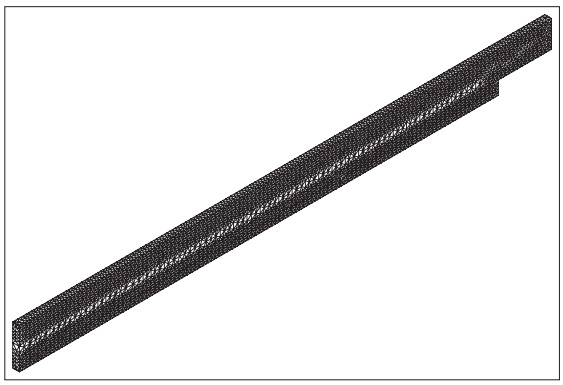

(a)

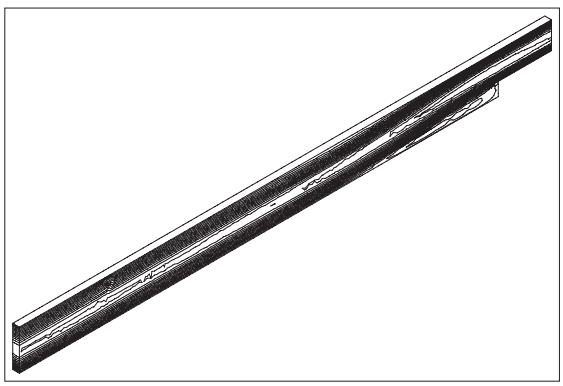

(b)

Figure 7. Flow over a backward facing step. Finite element mesh and u_1 velocity contours, (a) finite element mesh, (b) u_1 velocity contours.

All four confinement walls are assumed to be slip walls with normal velocity equal to zero. The inlet velocity is assumed to be uniform and the no-slip condition prevails on the sphere surface. This problem is solved using the fully explicit form of the CBS scheme.

For this problem, coarse, medium, and fine unstructured grids containing 271 680, 475 067 and 953 025 tetrahedral elements respectively have been generated. Figure 9 shows a portion of the fine grid along with the section on the symmetry plane. Figure 10 shows the contours of the u_1 component of the velocity computed on the fine grid for a Reynolds number of 100, and compares the C_p values on the surface along the flow axis with those available in literature. The non-dimensional C_p is calculated as

$$C_p = 2(p - p_{\text{ref}}) \tag{27}$$

with p_{ref} being the pressure at inlet. Figure 11 shows similar results for a Reynolds number of 200. The C_p comparisons are generally good and show the improvements achieved in the accuracy of the solution as the grid is refined.

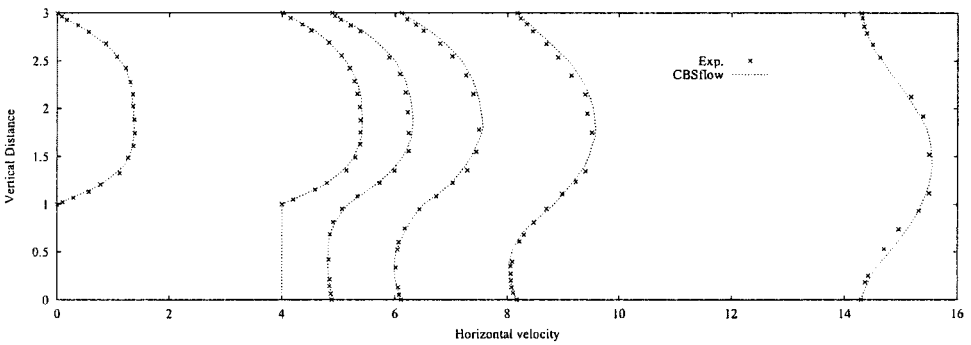

Figure 8. Flow over a backward facing step. Comparison of velocity distribution with experimental data [43].

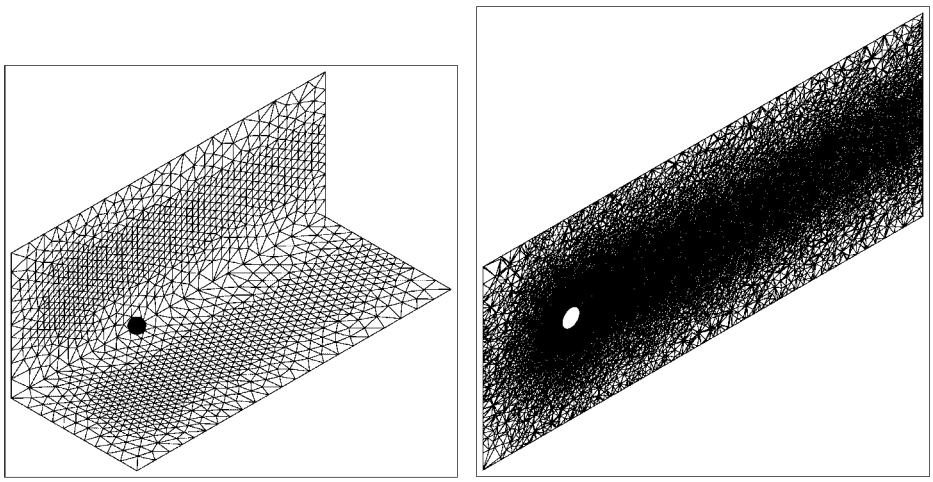

Figure 9. Unstructured grid for sphere, (a) Surface gird, (b) Symmetry plane sectional grid.

Note that the results used for comparison were generated using very fine structured meshes [44, 45]. It should also be noted that all the results differ from each other close to separation zone.

7.2. Non-isothermal flows

7.2.1. Buoyancy-driven flow in a cavity filled with single phase fluid. Some results are presented for the natural convection in a cubical thermal cavity, with insulated horizontal walls and prescribed temperature on two of the opposite vertical walls, with a different temperature on each wall. The flow condition on all these walls is assumed to be no-slip. The remaining two vertical walls have a zero flux flow and temperature conditions prescribed on them. This

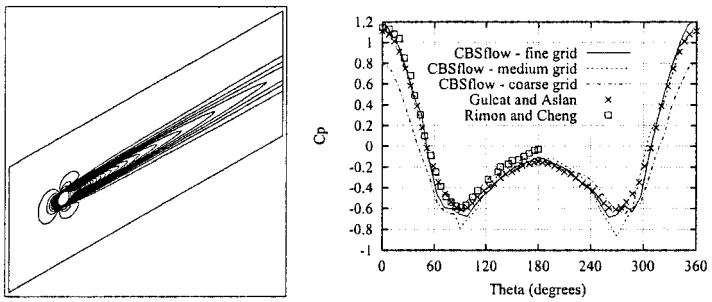

Figure 10. Flow past a sphere, $Re = 100$, (a) u_1 contours, (b) C_p comparison.

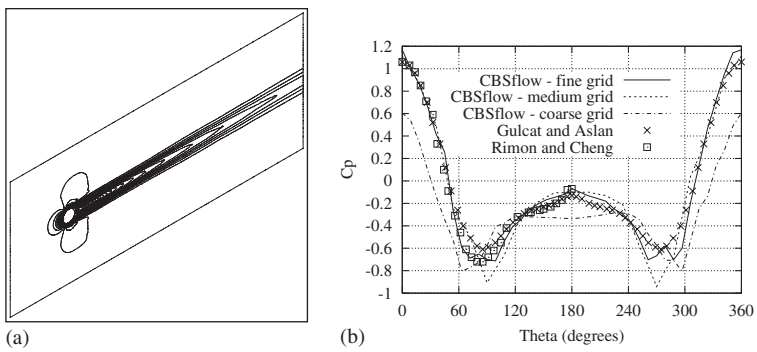

Figure 11. Flow past a sphere, $Re = 200$, (a) u_1 contours, (b) C_p comparison.

buoyancy-driven flow problem is a good test case because it contains regions of both highly diffusive and highly convective flow. The semi-implicit form of the solution procedure has been employed here.

The unstructured grid used for the computations is the one shown earlier in Figure 2.

Plate 1 shows the computed solutions for the flow with Rayleigh numbers of 10^5 and 10^6. The temperature contours are generally quite smooth and show the correct qualitative behaviour which is similar to that of the benchmark solutions [46]. As the Rayleigh number increases, the isotherms get increasingly packed near the vertical walls of the cavity, as expected.

Benchmark numerical solutions for the two-dimensional version of this problem are available in the literature [46], and Table I compares the maximum horizontal velocity u_1, the maximum vertical velocity u_3 and the average Nusselt number at the hot wall. The present results are in excellent agreement with the benchmark solution.

7.2.2. Buoyancy-driven flow in a cavity filled with fluid saturated porous medium. We now look at the natural convection in a thermal cavity containing a porous medium for which

Table I. Comparison with benchmark solution [46].

Ra	$u_{1\,\max}$	Reference [46]	$u_{3\,\max}$	Reference [46]	Nu	Reference [46]
10^3	3.574	3.649	3.725	3.697	1.225	1.116
10^4	18.123	16.178	21.973	19.617	2.364	2.243
10^5	36.389	34.73	74.524	68.59	4.493	4.517
10^6	65.02	64.63	217.274	219.36	8.855	8.797

Table II. Comparison of results for porous medium computations.

Flow conditions	$u_{3\,\max}$	Reference [36]
$Da = 10^{-6}$, $Ra = 10^8$, $\varepsilon = 0.8$	43.12	47.37
$Da = 10^{-2}$, $Ra = 10^4$, $\varepsilon = 0.8$	10.05	9.34

$\varepsilon = 0.8$. The definition of the problem is identical to the buoyancy-driven flow of single phase fluid discussed in the previous example. The mesh used in the previous example has again been employed here.

Plate 2 shows the flow with a Darcy number of 10^{-6}, Rayleigh number of 10^8 (Darcy flow regime) and also shows the flow with a Darcy number of 10^{-2}, Rayleigh number of 10^4 (non-Darcy flow regime). In both the cases presented, the Darcy–Rayleigh ($Da\,Ra$) number is identical. The Darcy–Rayleigh number is assumed to be equal in order to show the Darcy and non-Darcy effects. It should be noted that the Darcy–Rayleigh number is the only parameter governing the flow apart from the Prandtl number when the Darcy model is used [36].

The temperature contours are quite smooth and qualitatively match the results available in literature [36]. The flow at the lower Darcy number ($Da = 10^{-6}$) shows less convective mixing inside the cavity with a packing of the isotherms near the vertical walls of the cavity. The symmetry of the flow and temperature patterns at $Da = 10^{-6}$ shows the signs of un-symmetric developments. Establishing the steady state solution was difficult in this problem and this may be due to the high Rayleigh number used. It is possible that both three-dimensional and high Rayleigh number effects contributed to the minor un-symmetric pattern at this Darcy number. It is however noted that at $Da = 10^{-2}$ the pattern is symmetric with respect to the vertical centreline.

Table II compares the maximum vertical velocity obtained in the present calculations with those reported for a two-dimensional problem [36]. As seen the results differ a small amount from the two-dimensional results computed on structured meshes. These differences may be attributed to the three-dimensional effects, which are present in the present solution.

7.3. Transient flow

7.3.1. Vortex shedding behind a circular cylinder. The ability of the CBS scheme in its explicit form to simulate transient flow is illustrated by computing the vortex shedding in the wake of a circular cylinder. An unstructured grid containing 606 769 tetrahedral elements is employed. The computational domain is a rectangular box of length $20D$, where D is the diameter of the cylinder, with the downstream boundary located $16D$ from the centre

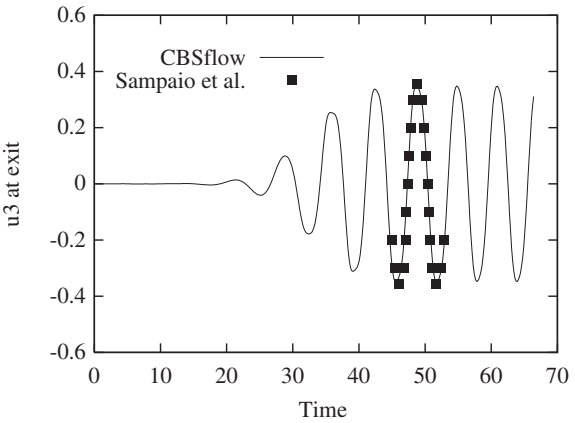

Figure 12. Vertical velocity in wake of circular cylinder, $Re = 100$.

of the cylinder. The top and bottom walls are located at a distance of $4D$ from the centre of the cylinder, while the side walls are $0.5D$ apart. The inlet velocity to the domain is assumed to be uniform and all the side walls are assumed to be slip walls. The cylinder surface is assumed to be solid and no-slip conditions are applied.

Plate 3 shows the grid and the contours of the u_1 component of the velocity at a Reynolds number of 100, plotted at a real time of 66.4. Figure 12 shows the variation of the vertical velocity with real time at the down-stream boundary point at the central horizontal line. The results obtained by de Sampaio *et al.* [47] are also shown and the agreement between the present results and adapted mesh solution of de Sampaio *et al.* is seen to be excellent.

7.3.2. Transient flow past a sphere. The unsteady flow past a three-dimensional body like a sphere is extremely complex and is therefore of great interest. The mesh employed here is the medium one used for the steady flow computations described earlier. The problem definition is identical to that discussed previously for steady flow past a sphere. Plate 4 shows the u_1 contours at a Reynolds number of 600 and at a real time of 75, where the unsteady nature of the wake is apparent and Figure 13 shows the variation of the u_2 velocity component at a downstream boundary node at the central horizontal line with real time.

A detailed numerical study of laminar flow past a sphere is recently presented by Lee [48] for Reynolds number of up to 500. It is clear from the available studies that the periodic vortex shedding, similar to the one for circular cylinder, exists for Reynolds numbers above 400. However, the periodic nature changes to a distinctive pattern similar to the one shown in Figure 13 beyond a Reynolds number of 500. The present results for a Reynolds number 600 confirms such a distinctive pattern.

7.4. Flow past multiple spheres in a channel

The microscopic approach to the analysis of flow in porous media involves modelling the problem as a collection of closely packed spheres. In this paper, such a problem is solved in order to show that the CBS scheme is capable of handling complicated domains and flow

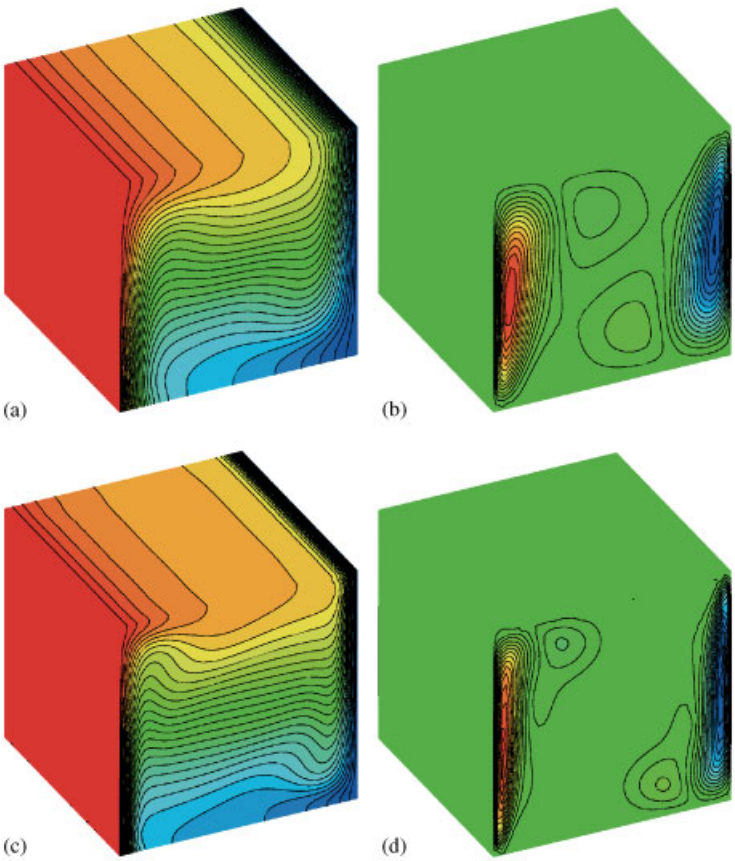

Plate 1. Buoyancy-driven flow in a cube with single phase fluid, (a) temperature contours, $Ra = 10^5$, (b) u_3 contours, $Ra = 10^5$, (c) temperature contours, $Ra = 10^6$, (d) u_3 contours, $Ra = 10^6$.

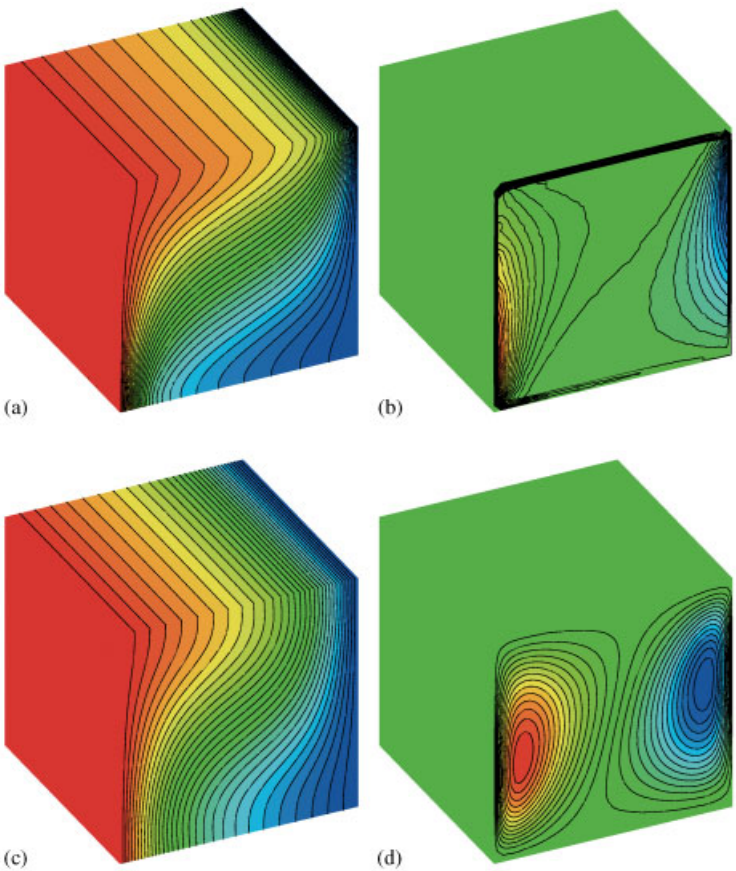

Plate 2. Buoyancy-driven flow in a cube with a porous medium, $\varepsilon = 0.8$, (a) temperature contours $Da = 10^{-5}$, $Ra = 10^{8}$, (b) u_3 contours $Da = 10^{-6}$, $Ra = 10^{8}$, (c) temperature contours $Da = 10^{-2}$, $Ra = 10^{4}$, (d) u_3 contours $Da = 10^{-2}$, $Ra = 10^{4}$.

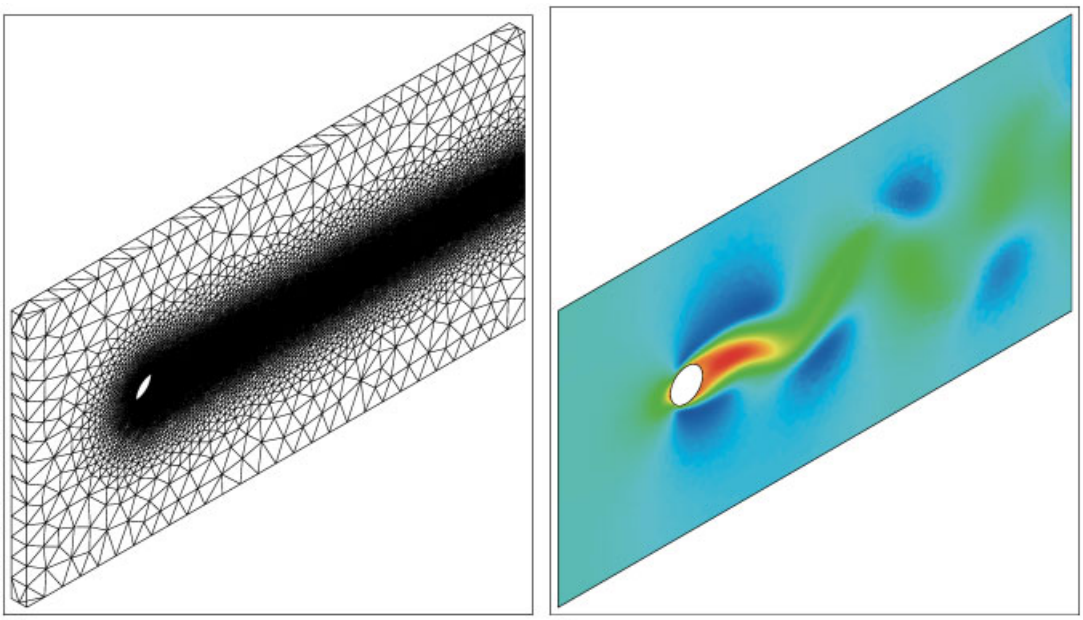

Plate 3. Unsteady flow past a circular cylinder, $Re = 100$, (a) surface grid, (b) u_1 contours on symmetry plane.

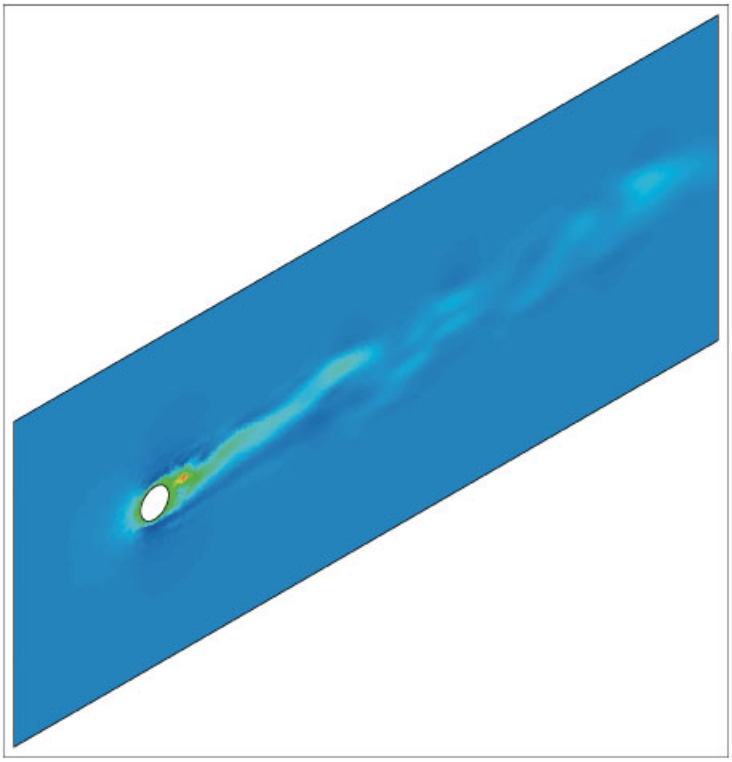

Plate 4. u_1 contours for unsteady flow past a sphere, $Re = 600$.

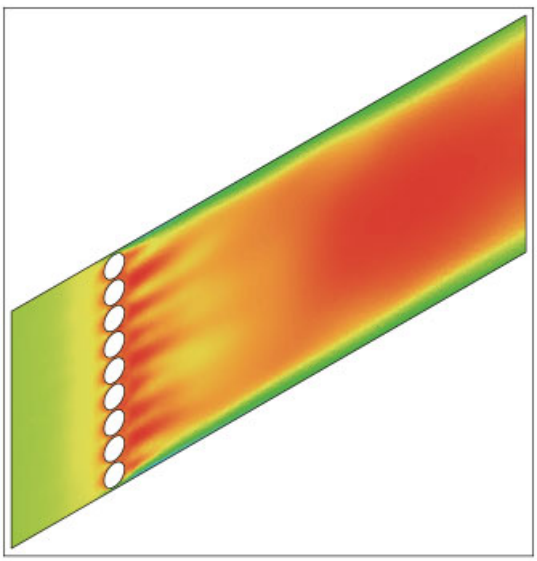

Plate 5. u_1 contours for flow past multiple spheres, $Re = 50$.

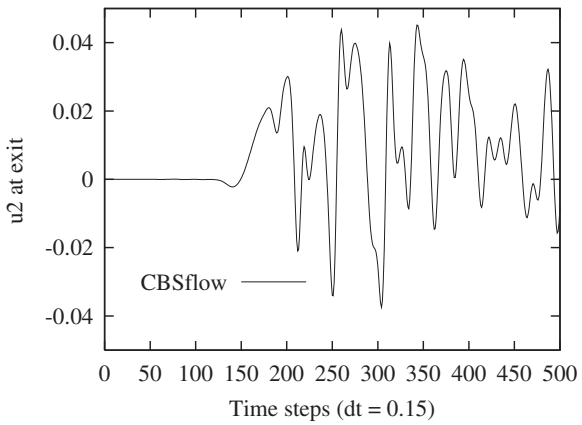

Figure 13. Vertical velocity in wake of sphere, $Re = 600$.

in this type of paths. Studying the flow past geometry is important in applications such as packed beds, electronic cooling arrangements and filter beds, where the particle based Reynolds numbers are normally small and the CBS scheme is an excellent choice for such conditions.

Here, we study the flow at $Re = 50$ past a 9×5 array of spheres in a channel. The channel is of length $25D$, where D is the sphere diameter, with the downstream boundary located at a distance of $20D$ from the centres of the spheres. The centre to centre distances between two spheres is taken to be equal to $1.1D$. The distance between the centre of the sphere closest to wall and the wall is equal to $0.6D$ for the top and bottom walls and $0.8D$ for the side walls.

The problem is solved for two different channel wall boundary conditions. In the first case, all the side walls, except the inlet and exit, surfaces are assumed to be slip walls. In the second case, two of the side walls (top and bottom) are assumed to be solid and noslip conditions are assumed on them. The other boundary conditions include uniform inlet velocity at inlet and no-slip conditions on the sphere surfaces.

Figure 14 shows a portion of the grid along with the section on the symmetry plane. The mesh is fine in the vicinity of the spheres to improve the accuracy of the simulation.

Plate 5 shows the contours of the u_1 component of the velocity at a Reynolds number of 50 along the mid-section for the first case. It can be observed that the results are fairly symmetric along the centre line as expected. It is also seen that each sphere develops its own back zones and that these zones interact with each other. This interaction and the interaction with the walls, make this problem interesting. It should be noted that the wake behind the spheres closest to the walls develop due to interaction between the spheres and the solid wall.

Figures 15 and 16 shows the C_p distribution on the spheres at different vertical positions on the central line for the two cases. In Figure 15, between $z = -2.2$ and 2.2, the c_p values are close to each other as expected. However, either the spheres at $z = -4.4$ or at 4.4, the interaction of the flow with the slip wall at bottom and top, respectively, increases the magnitude of c_p value dramatically along one half of the sphere surface. Note that such a deviation is not very high when the slip walls are replaced with solid walls, as shown in Figure 16.

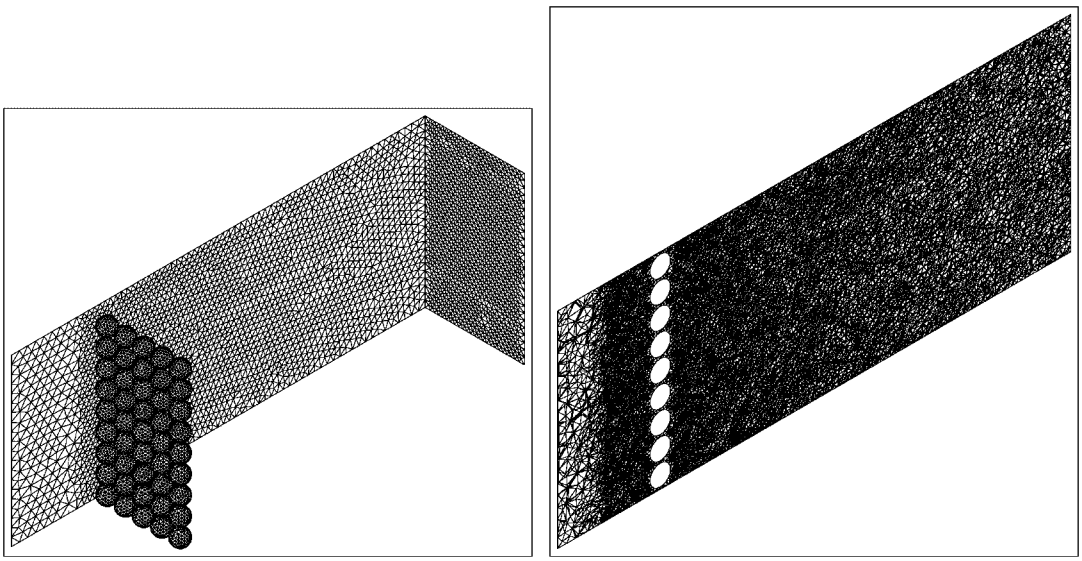

Figure 14. Unstructured grid for multiple spheres, (a) surface grid, (b) symmetry plane sectional grid.

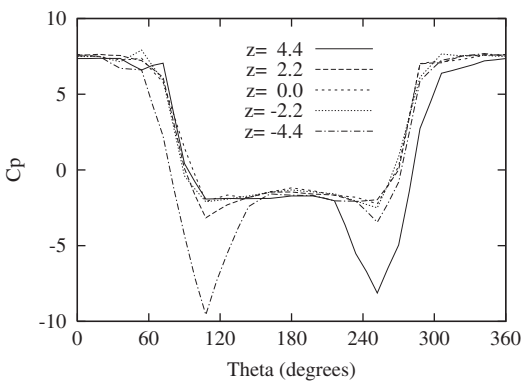

Figure 15. C_p distribution on the spheres at different vertical positions. With symmetry walls on all four sides.

8. CONCLUSIONS

In this paper, a number of incompressible flow problems have been solved in three dimensions for both steady and transient incompressible flow states. The potential for the use of CBS scheme for other incompressible flow applications is very good. Further studies are necessary in order to extend the scheme for problems such as viscoelastic flows and other non-Newtonian flows, such as blood flow in a human body.

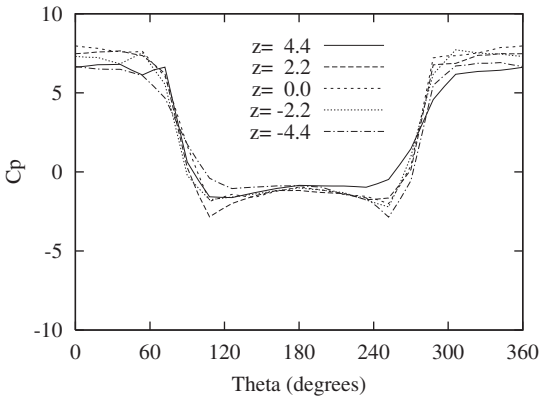

Figure 16. C_p distribution on the spheres at different vertical positions. With top and bottom solid walls.

ACKNOWLEDGEMENTS

This research is funded by EPSRC through grant GR/R29321/01. J. S. Mathur thanks the Director, National Aerospace Laboratories, Bangalore, India and the Council of Scientific & Industrial Research, India, for the grant of sabbatical leave and permission to work in the University of Wales Swansea.

REFERENCES

1. Morgan K, Peraire J. Unstructured grid finite element methods for fluid mechanics. *Reports on Progress in Physics* 1998; **61**:569–638.
2. Sorensen KA, Hassan O, Morgan K, Weatherill NP. Agglomerated multigrid on hybrid unstructured meshes for compressible flow. *International Journal for Numerical Methods in Fluids* 2002; **40**:593–603.
3. Tezduyar TE, Finite element methods for flow problems with moving boundaries and interfaces. *Archives of Computational Mechanics in Engineering* 2001; **8**:83–130.
4. Lanteri S. Parallel solutions of compressible flows using overlapping and non-overlapping mesh partitioning strategies. *Parallel Computing* 1996; **22**:943–968.
5. Weatherill NP, Hassan O, Morgan K, Jones JW, Larwood B. Towards fully parallel aerospace simulations on unstructured meshes. *Engineering Computations* 2001; **18**:347–375.
6. Morgan K, Weatherill NP, Hassan O, Brookes PJ, Said R, Jones J. A parallel framework for multidisciplinary aerospace engineering simulations using unstructured meshes. *International Journal for Numerical Methods in Fluids* 1999; **31**:159–173.
7. Moinier P, Giles MB. Stability analysis of preconditioned approximations of the Euler equations on unstructured meshes. *Journal of Computational Physics* 2002; **178**:498–519.
8. Löhner R. *Applied CFD Techniques.* Wiley: New York, 2001.
9. Zienkiewicz OC, Taylor RL. The finite element method. *Fluid Dynamics* (5th edn), vol. 3. Butterworth-Heinemann: London, 2000.
10. Weatherill NP, Turner-Smith EA, Jones J, Morgan K, Hassan O. An integrated software environment for multi-disciplinary computational engineering. *Engineering Computations* 1999; **16**:913–933.
11. Chorin AJ. Numerical solution of the Navier–Stokes equations. *Mathematics of Computation* 1968; **23**:341–354.
12. Comini G, Del Guidice S. Finite element solution of incompressible Navier–Stokes equations. *Numerical Heat Transfer*, *Part A* 1972; **5**:463–478.
13. Ramaswamy B. Finite element solution for advection and natural convection flows. *Computers and Fluids* 1988; **16**:349–388.
14. Ramaswamy B, Jue TC, Akin JE. Semi-implicit and explicit finite element schemes for coupled fluid thermal problems. *International Journal for Numerical Methods in Engineering* 1992; **34**:675–696.
15. Gresho PM, Sani RL. *Incompressible Flow and the Finite Element Method.* Wiley: New York, 2000.
16. Zienkiewicz OC, Codina R. A general algorithm for compressible and incompressible flow, Part I: The split characteristic based scheme. *International Journal for Numerical Methods in Fluids* 1995; **20**:869–885.

17. Zienkiewicz OC, Satya Sai BVK, Morgan K, Codina R, Vázquez M. A general algorithm for compressible and incompressible flow—Part II: tests on the explicit form. *International Journal for Numerical Methods in Fluids* 1995; **20**:887–913.
18. Codina R, Vázquez M, Zienkiewicz OC. A general algorithm for compressible and incompressible flows. Part III: The semi-implicit form. *International Journal for Numerical Methods in Fluids* 1998; **27**:13–32.
19. Zienkiewicz OC, Sai BVKS, Morgan K, Codina R. Split, characteristic based semi-implicit algorithm for laminar/turbulent incompressible flows. *International Journal for Numerical Methods in Fluids* 1996; **23**: 787–809.
20. Zienkiewicz OC, Nithiarasu P, Codina R, Vázquez M, Ortiz P. The characteristic-based-split procedure: An efficient and accurate algorithm for fluid problems. *International Journal for Numerical Methods in Fluids* 1999; **31**:359–392.
21. Zienkiewicz OC, Nithiarasu P. A universal algorithm for fluid dynamics. The characteristic based split (CBS) procedure. Some tests on stability and boundary conditions. *Archives of Mechanics* 2000; **52**:857–887.
22. Nithiarasu P, Zienkiewicz OC. On stabilization of the CBS algorithm. Internal and external time steps. *International Journal for Numerical Methods in Engineering* 2000; **48**:875–880.
23. Nithiarasu P. On boundary conditions of the characteristic based split (CBS) algorithm for fluid dynamics. *International Journal for Numerical Methods in Engineering* 2002; **54**:523–536.
24. Massarotti N, Nithiarasu P, Zienkiewicz OC. Characteristic-based-split (CBS) algorithm for incompressible flow problems with heat transfer. *International Journal of Numerical Methods for Heat and Fluid Flow* 1998; **8**: 969–990.
25. Nithiarasu P. An efficient artificial compressibility (AC) method based on the characteristic based split (CBS) method for incompressible flows. *International Journal for Numerical Methods in Engineering* 2003; **56**: 1815–1845.
26. Turkel E. Review of preconditioning methods for fluid dynamics. *Applied Numerical Mathematics* 1993; **12**: 257–284.
27. Weiss JW, Smith WA. Preconditioning applied to variable and constant density flows. *AIAA Journal* 1995; **33**:2050–2057.
28. Choi YH, Merkle CL. The application of preconditioning in viscous flows. *Journal of Computational Physics* 1993; **105**:207–223.
29. Turkel E. Preconditioning methods for solving the incompressible and low speed compressible equations. *Journal of Computational Physics* 1987; **72**:227–298.
30. Gaitonde AL. A dual time method for two dimensional incompressible flow calculations. *International Journal for Numerical Methods in Engineering* 1998; **41**:1153–1166.
31. Malan AG, Lewis RW, Nithiarasu P. An improved unsteady, unstructured, artificial compressibility, finite volume scheme for viscous incompressible flows: part I. Theory and implementation. *International Journal for Numerical Methods in Engineering* 2002; **54**:695–714.
32. Whitaker S. Diffusion and dispersion in porous media. *AIChE Journal* 1961; **13**:420–427.
33. Vafai K, Tien CL. Boundary and inertia effects on flow and heat transfer in porous media. *International Journal of Heat and Mass Transfer* 1981; **24**:195–203.
34. Hsu CT, Cheng P. Thermal dispersion in a porous medium. *International Journal of Heat and Mass Transfer* 1990; **33**:1587–1597.
35. Nithiarasu P, Seetharamu KN, Sundararajan T. Double-diffusive natural convection in an enclosure filled with fluid saturated porous medium—a generalised non-Darcy approach. *Numerical Heat Transfer*, *Part A* 1996; **30**:413–426.
36. Nithiarasu P, Seetharamu KN, Sundararajan T. Natural convective heat transfer in a fluid saturated variable porosity medium. *International Journal of Heat and Mass Transfer* 1997; **40**:3955–3967.
37. Nithiarasu P, Ravindran K. A new semi-implicit time stepping procedure for buoyancy driven flow in a fluid saturated porous medium. *Computer Methods in Applied Mechanics and Engineering* 1998; **165**:147–154.
38. Nithiarasu P, Seetharamu KN, Sundararajan T. Finite element modelling of flow, heat and mass transfer in fluid saturated porous media. *Archives of Computational Methods in Engineering*, *State of the art reviews* 2002; **9**:3–42.
39. Nithiarasu P. A comparative study on the performance of two time stepping schemes for convection in a fluid saturated porous medium. *International Journal for Numerical Methods in Heat and Fluid Flow* 2001; **11**: 308–328.
40. Massarotti N, Nithiarasu P, Zienkiewicz OC. Natural convection in porous medium-fluid interface problems—a finite element analysis by using the CBS procedure. *International Journal for Numerical Methods in Heat and Fluid flow* 2001; **11**:473–490.
41. Nithiarasu P, Seetharamu KN, Sundararajan T. Finite element analysis of transient natural convection in an odd-shapped enclosure. *International Journal for Numerical Methods in Heat and Fluid Flow* 1998; **8**: 199–216.
42. Ghia U, Ghia KN, Shin CT. High-Re solutions for incompressible flow using the Navier–Stokes equations and multigrid method. *Journal of Computational Physics* 1982; **48**:387–411.

43. Denham MK, Patrik MA. Laminar flow over a downstream-facing step in a two-dimensional flow channel. *Transactions of the Institution of Chemical Engineers* 1974; **52**:361–367.
44. Gülçat Ü, Aslan AR. Accurate 3D viscous incompressible flow calculations with FEM. *International Journal for Numerical Methods in Fluids* 1997; **25**:985–1001.
45. Rimon Y, Cheng SI. Numerical solution of a uniform flow over a sphere at intermediate Reynolds numbers. *The Physics of Fluids* 1969; **12**:949–959.
46. Davis G de V. Natural convection of air in a square cavity: a bench mark numerical solution. *International Journal for Numerical Methods in Fluids* 1983; **3**:249–264.
47. de Sampaio PAB, Lyra PRM, Morgan K, Weatherill NP. Petrov–Galerkin solutions of the incompressible Navier–Stokes equations in primitive variables in with adaptive remeshing. *Computer Methods in Applied Mechanics and Engineering* 1993; **106**:143–178.
48. Lee S. A numerical study of the unsteady wake behind a sphere in a uniform flow at moderate Reynolds numbers. *Computers and Fluids* 2000; **29**:639–667.
49. Malan AG, Lewis RW, Nithiarasu P. An improved unsteady, unstructured, artificial compressibility, finite volume scheme for viscous incompressible flows: part II. Application. *International Journal for Numerical Methods in Engineering* 2002; **54**:715–729.
50. Kim J, Moin P. Application of a fractional step method to incompressible Navier–Stokes equations. *Journal of Computational Physics* 1985; **59**:308–323.

